PHYSICAL REVIEW FLUIDS **2**, 094005 (2017)

Viscous free-surface flows on rotating elliptical cylinders

Weihua Li,[1] Marcio S. Carvalho,[2] and Satish Kumar[1,*]
[1]*Department of Chemical Engineering and Materials Science, University of Minnesota, Minneapolis, Minnesota 55455, USA*
[2]*Department of Mechanical Engineering, Pontificia Universidade Catòlica do Rio de Janeiro, Rio de Janeiro, RJ 22451-900, Brazil*
(Received 12 April 2017; published 22 September 2017)

The flow of liquid films on rotating discrete objects having complicated cross sections is encountered in coating processes for a broad variety of products. To advance fundamental understanding of this problem, we study viscous free-surface flows on rotating elliptical cylinders by solving the governing equations in a rotating reference frame using the Galerkin finite-element method. Results of our simulations agree well with Hunt's maximum-load condition [Hunt, Numer. Methods Partial Differ. Eqs. **24**, 1094 (2008)], which was obtained in the absence of surface tension and inertia. The simulations are also used to track the transient behavior of the free surface. For $O(1)$ cylinder aspect ratios, cylinder rotation results in a droplike liquid bulge hanging on the upward-moving side of the cylinder. This bulge shrinks in size due to surface tension provided that the liquid load is smaller than a critical value, leaving a relatively smooth coating on the cylinder. A decrease in cylinder aspect ratio leads to larger gradients in film thickness, but enhances the rate of bulge shrinkage and thus shortens the time required to obtain a smooth coating. Moreover, with a suitably chosen time-dependent rotation rate, more liquid can be supported by the cylinder relative to the constant-rotation-rate case. For cylinders with even smaller aspect ratios, film rupture and liquid shedding may occur over the cylinder tips, so simultaneous drying and rotation along with the introduction of Marangoni stresses will likely be especially important for obtaining a smooth coating.

DOI: 10.1103/PhysRevFluids.2.094005

I. INTRODUCTION

The flow of liquid films on nonflat substrates plays a central role in the manufacturing of products such as biomedical devices, automobiles, and food. These products, which represent nonflat substrates, often require a coating on them for purposes such as protection and appearance. The coating is formed by depositing one or several liquid layers onto the substrate and then solidifying the resulting film through drying. The final film thickness usually needs to lie within a specified range for the product to exhibit desired properties. However, controlling film thickness over a nonflat substrate is a challenging task not only due to surface curvature, but also due to the possible presence of object rotation.

The most commonly studied model geometry is that of a circular cylinder rotating about its horizontal axis [1,2]. Moffatt [1] first considered this problem in the thin-film limit in the absence of both surface tension and inertia. In his pioneering work, he provided an analytical expression for the maximum supportable load (A_m^{Circular}) on a rotating cylinder, which can be written as

$$A_m^{\text{Circular}} = 1.057\left(\frac{4\pi}{3}\right)\gamma^{-1/2}, \tag{1}$$

where $\gamma = ga\rho/\mu\Omega$ is the Stokes number, measuring the importance of gravitational forces relative to viscous forces. Here a is the cylinder radius, ρ is the liquid density, g is the magnitude of the

*Corresponding author: kumar030@umn.edu

gravitational acceleration, μ is the liquid viscosity, and Ω is the cylinder rotation rate. The maximum load can be interpreted as a maximum volume (or mass) of liquid per unit length of the cylinder [in Eq. (1), A_m has been made dimensionless with respect to a^2].

For a cylinder having load $A < A_m^{\text{Circular}}$, the cylinder can support the liquid, and a so-called Moffatt-type smooth coating can be obtained in which there is a thicker film on the upward-moving side of the cylinder and a thinner film on the downward-moving side of the cylinder. Kelmanson [3] refined Moffatt's maximum load condition (1) by selectively retaining some higher-order terms that were not included in Moffatt's work.

For a cylinder having load $A > A_m^{\text{Circular}}$, no analytical solution exists in Moffatt's model since the film tends to sag under the action of gravity. Evans *et al.* [4] have extended Moffatt's model to include surface tension. Numerical solutions of their model show that surface tension tends to support the excess liquid when $A > A_m^{\text{Circular}}$, giving rise to a droplike liquid bulge hanging from the underside of the cylinder. Experimental investigations of the maximum-supportable-load condition have been undertaken by Kelmanson [3] and Preziosi and Joseph [5], and their results are in reasonable agreement with Moffatt's approximate criterion.

In many applications, such as the production of orthopedic implants [6], metal tubes [7], and food bars [8], the objects to be coated do not have a circular cross section. For these products, curvature variations along the circumference may trigger capillary flows that drive liquid from areas of high to low curvature. The resulting phenomena, including film rupture near sharp corners and uneven liquid and solute distribution, have the potential to adversely influence the quality of the final coating. Limited knowledge about the complex interplay between surface tension, gravity, and rotation in liquid-film flow on objects with noncircular cross sections hinders the design and optimization of coating processes for these objects.

The influence of noncircular cross sections on coating flows on rotating objects was first studied by Hunt [9]. He considered two-dimensional Stokes flow on the exterior of an elliptical cylinder rotating with uniform angular speed about the center of the ellipse. Neglecting the effects of surface tension, he solved the full Stokes equations numerically and showed that the maximum amount of liquid that can be supported by an elliptical cylinder ($A_m^{\text{Elliptical}}$) is less than that in the circular case (A_m^{Circular}). In both cases, the maximum load decreases as the Stokes number increases (which corresponds to stronger effects of gravity), with approximately the same power-law dependence. Steady solutions were not found on an elliptical cylinder, in contrast to the circular-cylinder case. However, there exist periodic solutions when $A < A_m^{\text{Elliptical}}$, in which the solution is repeated after one full revolution of the cylinder. The present paper extends the work of Ref. [9] to incorporate the effects of surface tension.

The governing equations and solution method are presented in Sec. II. Results are presented in Secs. III and IV for elliptical cylinders having $O(1)$ and $O(10^{-1})$ aspect ratios, respectively. We summarize our results and discuss the implications of our findings for coating of discrete objects in Sec. V.

II. MATHEMATICAL MODEL

We consider the free-surface flow of a Newtonian liquid with constant viscosity μ, density ρ, and surface tension σ on a rotating elliptical cylinder (Fig. 1). Our focus will be on the film-thickness evolution around the cylinder circumference, so thickness variations in the axial direction are neglected. The cylinder aspect ratio is $\alpha = b/a$, where a and b are the lengths of the semimajor and semiminor axes, respectively. The cylinder surface $\mathbf{R}(x_0, y_0)$ is located at

$$x_0 = e\cosh\zeta_0\cos\nu, \quad y_0 = e\sinh\zeta_0\sin\nu, \tag{2}$$

where $e = a/\cosh(\zeta_0)$, $\zeta_0 = \frac{1}{2}\ln[(a+b)/(a-b)]$, and $\nu \in [0,2\pi]$. The cylinder rotates about the center of the ellipse in the anticlockwise direction at angular speed Ω.

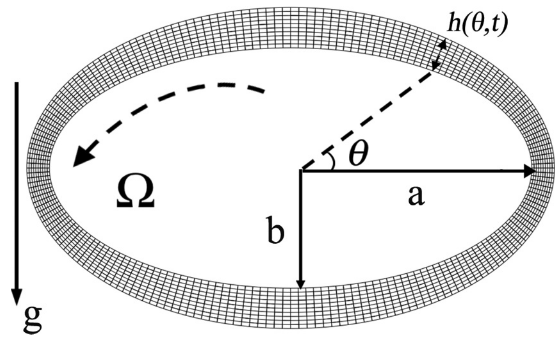

FIG. 1. Sample finite-element mesh at $t = 0$ for a liquid film on an elliptical cylinder.

A. Governing equations

We adopt a reference frame that rotates with the cylinder, and employ a Cartesian coordinate system with unit vectors $\mathbf{e}_x$, $\mathbf{e}_y$, and $\mathbf{e}_z$. The corresponding momentum conservation equation is [10]

$$\rho[\mathbf{u}_t + \mathbf{u} \cdot \nabla \mathbf{u}] = -\nabla p + \mu \nabla^2 \mathbf{u} - \rho \boldsymbol{\Omega} \times (\boldsymbol{\Omega} \times \mathbf{r}) - 2\rho \boldsymbol{\Omega} \times \mathbf{u} + \rho \mathbf{g}, \tag{3}$$

where p is pressure, $\mathbf{u}$ is the velocity vector, $\mathbf{g} = g\mathbf{e}_g = -g\sin(\Omega t)\mathbf{e}_x - g\cos(\Omega t)\mathbf{e}_y$ is the gravitational acceleration, $\boldsymbol{\Omega} = \Omega \boldsymbol{e}_z$ is the angular velocity vector, and $\mathbf{r}$ is the position vector of a fluid element.

Inspired by prior work on circular cylinders [4], we scale length with a, velocity with $U = \rho g a^2/\mu$, time with a/U, and pressure with $\mu U/a$. We can define two Reynolds numbers, $\mathrm{Re} = \rho^2 g a^3/\mu^2$, based on a gravitational drainage velocity (U), and $\mathrm{Re}_\Omega = \rho \Omega a^2/\mu$, based on the cylinder velocity ($a\Omega$). The scaled governing equations for mass and momentum conservation are

$$\nabla \cdot \mathbf{u} = 0, \tag{4}$$

$$\mathrm{Re}[\mathbf{u}_t + \mathbf{u} \cdot \nabla \mathbf{u}] = -\nabla p + \nabla^2 \mathbf{u} - W^2 \mathbf{r} - 2\mathrm{Re}_\Omega(\mathbf{e}_z \times \mathbf{u}) + \mathbf{e}_g, \tag{5}$$

where $W = \Omega/\sqrt{g/a}$ is the dimensionless rotation rate. Here $\mathbf{e}_g = -\sin(MWt)\mathbf{e}_x - \cos(MWt)\mathbf{e}_y$, where $M = \mu/\rho\sqrt{ga^3}$ is a dimensionless viscosity.

There are three inertia-related terms in Eq. (5): the standard inertial term ($\mathrm{Re}[\mathbf{u}_t + \mathbf{u} \cdot \nabla \mathbf{u}]$), the Coriolis term $[\mathrm{Re}_\Omega(\mathbf{e}_z \times \mathbf{u})]$, and the centrifugal term ($W^2\mathbf{r}$). The last of these terms arises from the standard inertial term in a stationary reference frame. Following Refs. [4,11], we focus on the effects of centrifugal forces and neglect the other two inertia-related terms. With these simplifications, Eq. (5) becomes

$$\mathbf{0} = -\nabla p + \nabla^2 \mathbf{u} - W^2 \mathbf{r} + \mathbf{e}_g. \tag{6}$$

The boundary conditions at the cylinder surface, $\mathbf{R}(x_0, y_0)$, are no-slip and no-penetration,

$$\mathbf{t} \cdot \mathbf{u} = 0, \quad \mathbf{n} \cdot \mathbf{u} = 0, \tag{7}$$

where $\mathbf{n}$ and $\mathbf{t}$ are the unit outward normal and tangent vectors. At the free surface, $\mathbf{r}_s(x, y)$, we have the kinematic and interfacial-stress boundary conditions,

$$\mathbf{n} \cdot \mathbf{u} = \mathbf{n} \cdot \dot{\mathbf{r}}_s, \tag{8}$$

$$\mathbf{n} \cdot \mathbf{T} = -\frac{\kappa}{\mathrm{Bo}} \mathbf{n}, \tag{9}$$

where $\mathbf{T}$ is the total stress tensor (the components of which are nondimensionalized by $\mu U/a$), $\kappa = \nabla_s \cdot \mathbf{n}$ is the surface curvature with ∇_s being the surface gradient operator, and $\dot{\mathbf{r}}_s$ is the

TABLE I. Order-of-magnitude estimates of dimensional quantities. The viscosity, density, and surface tension are representative of a glycerol-water mixture.

Constants	Typical values
Length of semimajor axis, a (cm)	1
Film thickness, H (cm)	0.1
Rotation rate, Ω (rad/s)	10^{-1}–10
Viscosity, μ (cP)	300
Density, ρ (g/cm^3)	1
Surface tension, σ (dyn/cm)	10–10^2

free-surface velocity. The Bond number, $\mathrm{Bo} = \rho g a^2/\sigma$, measures the importance of gravity relative to surface tension.

B. Parameter values

Order-of-magnitude estimates for key dimensional quantities are listed in Table I. As the applications that motivate this work involve thin coatings, the characteristic film thickness H is at least an order of magnitude smaller than the length of the semimajor axis a. This allows us to use lubrication theory to estimate the strength of inertial forces [12]. With lubrication scalings [4], the Reynolds number becomes $\mathrm{Re} = \rho g H^2 a/\mu^2$ while the definition of Re_Ω is unchanged, and notably, both of these parameters are multiplied by ϵ^2 in the governing equations, where $\epsilon = H/a$. For the parameter values given in Table I, $\epsilon^2\mathrm{Re}$ and $\epsilon^2\mathrm{Re}_\Omega$ are both no more than $O(10^{-1})$.

When lubrication scalings are used, the definition of W is unchanged, and it is not multiplied by any nonzero power of ϵ in the governing equations. For the parameter values given in Table I, W ranges from approximately 0.003 to 0.3. Because we are interested in thin films, we choose to retain the effects of centrifugal forces while neglecting inertial effects associated with Re and Re_Ω. This is consistent with the approach followed in Refs. [4,11] and leads to Eq. (6). This approximation is expected to be increasingly accurate as the film becomes thinner because of the ϵ^2 factor multiplying Re and Re_Ω.

While we cannot simulate thinner films than those considered here due to computational limitations (since the film rapidly becomes too thin in places to accurately resolve), by considering this limiting case we can gain insight into the behavior that would be expected for even thinner films. Moreover, by neglecting inertial effects associated with Re and Re_Ω, we can isolate the influence of centrifugal forces by studying the case where gravitational forces are absent (Secs. III A and IV A). Examination of this limiting case provides an important foundation for future work that includes the other inertial terms, which may become important for thicker films, less viscous liquids, and faster rotation rates, and lead to an even richer variety of behavior than what is observed here.

C. Solution method

Equations (4) and (6) with boundary conditions (7), (8), and (9) are solved with the Galerkin finite-element method (GFEM) [12,13]. Elliptic mesh generation is used to map the unknown flow domain (x,y) into a reference computational domain (ξ,η). A second-order adaptive time-stepping algorithm is used for time integration. At each time step, the following set of elliptic partial differential equations are solved simultaneously with the other equations in the computational domain:

$$\nabla \cdot (D_\xi \nabla \xi) = 0, \quad \nabla \cdot (D_\eta \nabla \eta) = 0, \tag{10}$$

where D_ξ and D_η are mesh diffusion coefficients used to distribute elements within the physical domain. The diffusion coefficients and boundary conditions for these equations are discussed in Ref. [14].

Following Hunt [9], we perform simulations with an initial coating shown in Fig. 1, whose inner surface is described by Eq. (2) and outer surface, $\mathbf{r}_s(x,y)$, is given by

$$x = e\cosh(\zeta_0 + \zeta)\cos\nu, \quad y = e\sinh(\zeta_0 + \zeta)\sin\nu. \tag{11}$$

Here the constant ζ determines the dimensionless load A_0 of fluid deposited onto the cylinder, which is taken to be the area between the cylinder surface and the free surface [9],

$$A_0 = \int_0^{2\pi} \frac{e^2}{4}\{\sinh[2(\zeta_0 + \zeta)] - \sinh(2\zeta_0) - 2\zeta\cos(2\nu)\}d\nu. \tag{12}$$

The quantity $\rho a^2 A_0$ gives the dimensional mass per unit length.

For the loads considered in this paper, the initial film thickness is typically $\sim$10%$-$20% of the length of the semimajor axis. While in principle the lubrication approximation could be applied to develop a simplified model equation [15], in practice this is cumbersome due to the complicated surface geometry. Our GFEM scheme also has the advantage of being applicable to objects with surfaces for which no analytical description is available.

For our calculations, 2000 elements (200 elements in the angular direction and 10 elements in the radial direction) were found to be sufficient. To ensure conservation of mass, we calculate the percent deviation of the liquid load using $\epsilon = 100(A_{\max} - A_{\min})/A_0$, where $A_{\max}$ and $A_{\min}$ are the maximum and minimum area during the entire calculation. Results of our simulations are considered accurate if $\epsilon < 0.1$ [13]. Typical computation times for a given run ranged from several days to 1 wk on a workstation with a 2.93 GHz Intel Core i7 processor.

For a fixed set of problem parameters (W, A_0, Bo, and α), we use the GFEM to numerically solve for the location of the free surface as a function of time. To track the film evolution, we then extract the film thickness, $h(\theta,t)$, as a function of time and the angular position, θ, in a reference frame rotating with the cylinder. The film thickness is measured in the direction normal to the cylinder surface from a point on the cylinder surface whose angular position is θ (Fig. 1).

III. RESULTS: $O(1)$ ASPECT RATIO

In this section, we consider elliptical cylinders with $O(1)$ aspect ratios ($0.5 \leqslant \alpha \leqslant 1$).

A. Zero-gravity case

We first consider the case where the cylinder rotates rapidly and the effects of gravity can be neglected. In this regime, the drainage rate can no longer be used as the characteristic velocity, so we rescale the governing equations (4) and (6) using σ/μ and σ/a as the new characteristic velocity and pressure (stress), respectively [12]. The resulting dimensionless governing equations become

$$\nabla \cdot \mathbf{u} = 0, \tag{13}$$

$$\mathbf{0} = -\nabla p + \nabla^2\mathbf{u} - \mathrm{We}\,\mathbf{r}, \tag{14}$$

where $\mathrm{We} = \rho\Omega^2 a^3/\sigma$ is the Weber number and provides a measure of the strength of centrifugal forces relative to surface-tension forces. Larger We corresponds to faster rotation rates and stronger centrifugal forces acting on the liquid.

For a circular cylinder ($\alpha = 1$), Evans *et al.* [4] showed that small perturbations to an initial film of uniform thickness tend to grow in amplitude under the action of centrifugal forces, leading to the formation of small droplets evenly spaced around the cylinder circumference. For a sufficiently thin initial film, the film will eventually reach a steady state in which the number of droplets, N, is a function of We and has the form

$$N = [\sqrt{(1 + \mathrm{We})/2}], \tag{15}$$

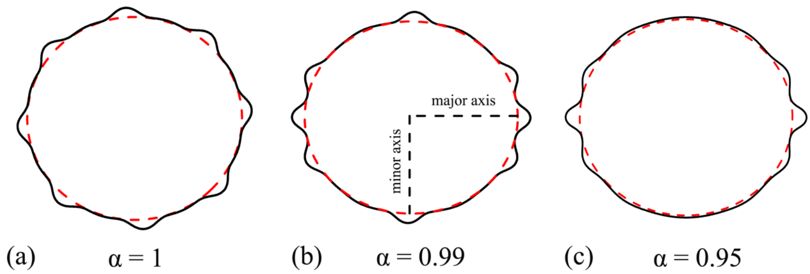

FIG. 2. Steady free-surface profiles on rotating cylinders with $A_0 = 0.2$ and We = 160 ($N = 8$) for three different values of the cylinder aspect ratio. The red dashed lines indicate the cylinder surface.

where $[x]$ is the greatest integer less than x. The time scale over which the steady state is reached (maximum growth rate) is proportional to $\sigma h_0^3(1 + \mathrm{We})^2/(3\mu a^4)$, where h_0 is the initial film thickness [4].

To investigate the case of elliptical cylinders, we solve Eqs. (13) and (14) numerically for different cylinder aspect ratios α. We pick an initial load $A_0 = 0.2$ and a rotation rate We = 160 as a representative case. Similar to the circular-cylinder case, a steady state (in the rotating reference frame) is reached; the resulting free-surface profiles are shown in Figs. 2(b) and 2(c) for $\alpha = 0.99$ and 0.95. The steady free-surface profile on a circular cylinder is shown in Fig. 2(a) for comparison. Steady states reported here and elsewhere in the paper are long-time solutions rather than direct solutions, and so should be regarded as apparent steady states.

For We = 160, the corresponding value of N calculated from Eq. (15) is eight. Figure 2(a) shows that eight droplets of almost the same size develop on the circular cylinder, and they are evenly spaced around the cylinder circumference and connected by very thin films. With a slight decrease in α [Fig. 2(b)], the number of droplets is still eight, but these droplets are unevenly spaced and some of the droplets tend to shift to the cylinder tips. As we further decrease α to a value of 0.95 [Fig. 2(c)], only six droplets develop on the elliptical cylinder, and the two droplets over the cylinder tips are much larger than the rest of the droplets.

Since stronger centrifugal forces acting on the liquid over the tips tend to draw liquid from surrounding areas, droplets are more stable near the tips, causing the uneven spacing between droplets in Figs. 2(b) and 2(c). A decrease in α strengthens the gradient in centrifugal forces, which produces two main droplets over the tips but greatly suppresses the growth of droplets in the surrounding areas. This explains the uneven droplet sizes and the decrease in the number of droplets in Fig. 2(c).

The influence of A_0 and We can be understood from Eq. (15) and the expression for the maximum growth rate given right after. Increasing the value of A_0 corresponds to having a larger initial film thickness, which means that steady states will be reached sooner. Increasing the value of We will have the same effect and will also lead to the formation of more droplets. We note that if the growth rate is too large, the droplets may grow into filaments and then break up into smaller droplets. However, simulations of this case require a very small time step size and a very high spatial resolution that are beyond our current computational capabilities.

For even smaller cylinder aspect ratios ($\alpha < 0.95$), the larger variation in substrate curvature leads to stronger capillary pressure gradients that tend to drive liquid away from the tips. Because this phenomenon is also seen with cylinders having small aspect ratios ($\alpha < 0.5$), we discuss it in Sec. IV A.

B. Gravity effects

For the case where gravitational effects are significant, Moffatt [1] developed an expression for the maximum load that can be supported on a rotating circular cylinder [Eq. (1)] in the thin-film regime. Kelmanson [3] proposed a refinement to Moffatt's criterion that selectively retains some higher-order terms and provided an explicit expression for the maximum load [Eq. (4.13) in Ref. [3]]. Both Moffatt and Kelmanson neglected the effects of surface tension and inertia in their work.

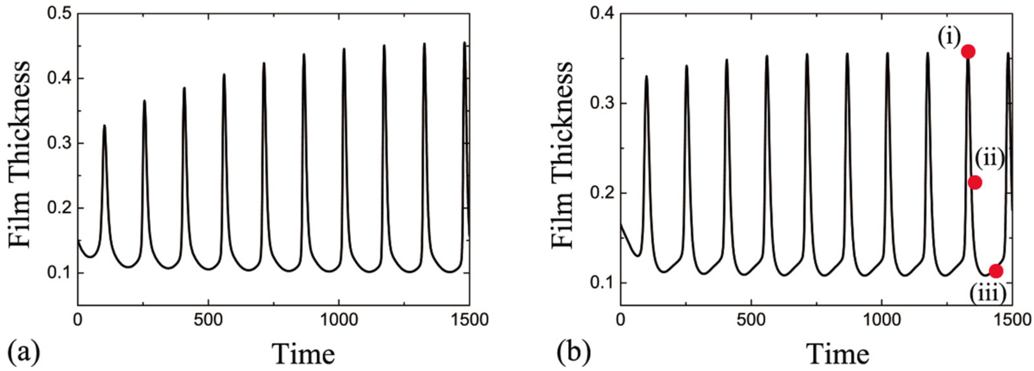

FIG. 3. Time variation of film thickness at $\theta = \pi/2$ with Bo = 12.5, $M = 0.1$, $W = 0.43$, and (a) $A_0 = 1$ and $\alpha = 1$ (circular cylinder), (b) $A_0 = 0.75$ and $\alpha = 0.5$. The corresponding free-surface profiles at times (i), (ii), and (iii) are shown in Fig. 4.

Evans *et al.* [4] used lubrication theory to derive a nonlinear evolution equation for the film thickness on a rotating circular cylinder in the presence of surface tension and centrifugal forces which was then solved numerically. To confirm Moffatt's criterion, they tracked the time evolution of the film thickness at a fixed point in space in a fixed reference frame.

For $A > A_m^{\text{Circular}}$ [Eq. (1)], excess liquid drains under the action of gravity and forms a droplike bulge on the cylinder underside, supported by surface tension. The film thickness there increases monotonically until the coating reaches a steady state within a few revolutions. For $A < A_m^{\text{Circular}}$, the droplike bulge rises over the cylinder symmetry plane and is carried around the cylinder in the direction of rotation. The rotation rate of the bulge is less than but comparable to the cylinder rotation rate [4]. Simultaneously, the bulge shrinks in size and the film approaches a Moffatt-type smooth coating (Sec. I) with a thicker film on the upward-moving side of the cylinder and a thinner film on the downward-moving side of the cylinder. As a consequence, the film thickness at a given point exhibits a decaying oscillation with roughly constant frequency (Fig. 7 in Ref. [4]).

Similar calculations are performed in this work to approximately determine the maximum load that can be supported by an elliptical cylinder. However, it is more convenient to track the film evolution at a fixed point on the cylinder surface in our model since we consider the problem in a rotating reference frame.

Based on the parameter values given in Table I, we set the dimensionless viscosity to $M = 0.1$. If lubrication scales are used (Sec. II B), the definition of the Bond number remains the same but it is multiplied by ϵ in the normal-stress balance [4]. The values in Table I then indicate that ϵBo ranges from $O(1)$–$O(10)$. Consistent with this, we choose a value of Bo = 12.5. For $O(1)$ values of Bo, the film tends to thin rapidly in areas of high substrate curvature due to the stronger surface-tension forces, and as a consequence, we are not able to accurately resolve the film evolution.

We choose a dimensionless rotation rate $W = 0.43$ as a representative case; this value is of the same order of magnitude as those given in Sec. II B. The corresponding maximum supportable load on a circular cylinder calculated from Kelmanson's criterion [3] is $A_m^{\text{Circular}} = 0.96$. Choosing smaller values of W would lead to smaller values of the maximum load. However, this can lead to computational problems for cases where the initial load is less than the maximum value since the film rapidly becomes too thin in places to accurately resolve. We note that for this value of W, centrifugal forces do not play an important role since that term is proportional to W^2 in Eq. (6). Indeed, results from selected runs we have performed neglecting the centrifugal term in Eq. (6) are not significantly different from those obtained when that term is included. The parameter W also determines the dimensionless rotation period of the cylinder, $2\pi/MW$ (Sec. II A).

Simulations were performed with $A_0 = 1 > A_m^{\text{Circular}}$ first. For a circular cylinder, we plot in Fig. 3(a) the time evolution of the film thickness at $\theta = \pi/2$ on the cylinder surface. For an elliptical

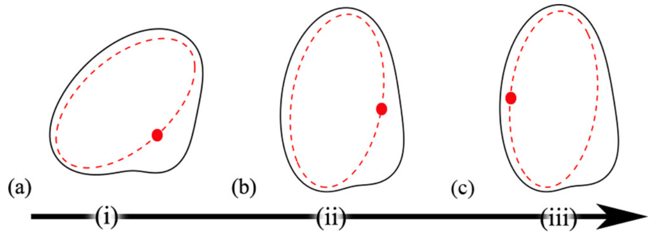

FIG. 4. Free-surface profiles on an elliptical cylinder at three given times [marked in Fig. 3(b)]. The red dots indicate the $\theta = \pi/2$ point on the cylinder surface.

cylinder with $\alpha = 0.5$, we found that the film thickness at the cylinder bottom grows rapidly and could no longer be resolved numerically after one revolution. To avoid this, we decreased A_0 (initial load) until a periodic state was reached where the coating restores its shape after every half-revolution. This occurred when $A_0 = 0.75$, and we show in Fig. 3(b) the time evolution of the film thickness at $\theta = \pi/2$.

For both the circular cylinder [Fig. 3(a)] and elliptical cylinder [Fig. 3(b)], the film thickness at $\theta = \pi/2$ oscillates with a fixed frequency. The amplitudes of the oscillations increase monotonically until they reach steady values at later times. Oscillations in both cases can be attributed to the formation of a liquid bulge, so we focus on the elliptical cylinder in the following discussion. We have selected several times during the later stage of the time evolution in Fig. 3(b) and plot the corresponding free-surface profiles in Fig. 4.

As seen in Fig. 4, excess liquid forms a droplike bulge, supported by surface tension, near the underside of the cylinder. As a result, the film thickness over $\theta = \pi/2$ reaches its maximum when this point rotates into the bulge area [Fig. 4(a)]. As more liquid is driven into the bulge due to gravity, it grows in size, which explains the increasing amplitude in Fig. 3(b). The coating reaches a quasisteady state where the free-surface shape changes periodically due to the variation in the cylinder orientation. The free-surface tends to restore its shape after every half-revolution as shown in Figs. 4(b) and 4(c).

To investigate the regime where the load A_0 is relatively low, we plot in Fig. 5 the time evolution of the film thickness at $\theta = \pi/2$ with $W = 0.43$ and $A_0 = 0.72 < A_m^{\text{Circular}}$ for three different values of α. For all of these three values, the film thickness at $\theta = \pi/2$ oscillates with a fixed frequency similar to the larger-load case (shown in Fig. 3). However, the oscillation amplitude does not grow monotonically with time, in contrast to the case where $A_0 > A_m^{\text{Elliptical}}$ (Fig. 3; note that $0.72 < A_m^{\text{Elliptical}} < 0.75$). For $\alpha = 1$ [Fig. 5(a)] and $\alpha = 0.8$ [Fig. 5(b)], the corresponding upper-envelope functions oscillate with decaying amplitudes, while for $\alpha = 0.5$ [Fig. 5(c)], the upper-envelope function decays almost monotonically, and the film reaches a quasisteady state at a much earlier time. These three cases are discussed below in more detail.

For a circular cylinder, the superposition of a shorter-period oscillation and a longer-period oscillation results in the time evolution of film thickness plotted in Fig. 5(a). To gain deeper insight, we show in Fig. 6(a) the enlargement of the boxed region in Fig. 5(a). Schematics of the free-surface profiles at three times [marked (I)–(III) in Fig. 6(a)] are shown in Fig. 6(b) to explain the mechanisms behind the shorter-period oscillation and the longer-period oscillation. Since the film-thickness variation at a fixed point is small relative to the thickness of the film, schematics rather than actual free-surface profiles are shown for ease of visualization.

Due to the effects of rotation and gravity, a coating on a rotating circular cylinder is thicker on the upward-moving side and thinner on the downward-moving side [1]. As a consequence, the film thickness at $\theta = \pi/2$ decreases as the $\theta = \pi/2$ point on the cylinder surface [red dots in Fig. 6(b)] rotates from the upward-moving side to the downward-moving side [from time (I) to time (II) in Fig. 6(b] and increases as the $\theta = \pi/2$ point rotates back to the upward-moving side. This is the origin of the shorter-period oscillation in film thickness. The oscillation period equals the time

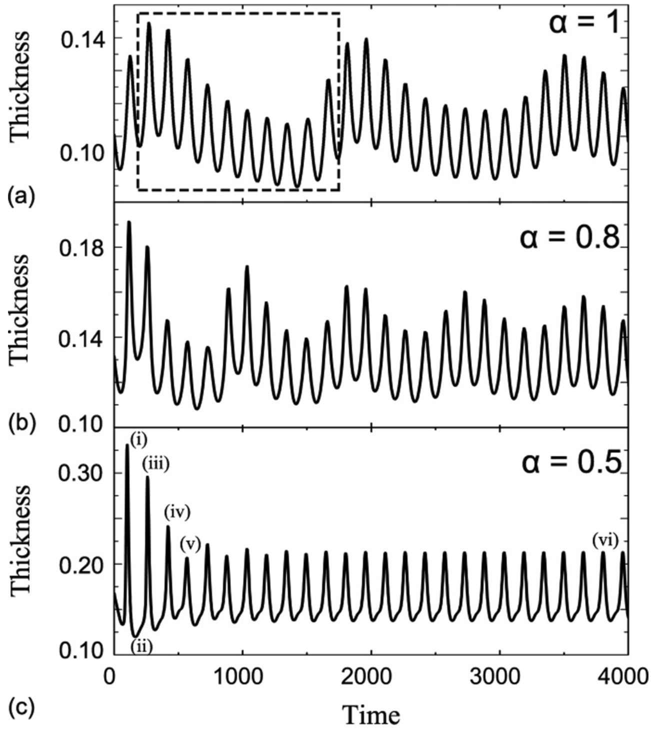

FIG. 5. Time variation of film thickness at $\theta = \pi/2$ with Bo $= 12.5$, $M = 0.1$, $W = 0.43$, and $A = 0.72$ for three different values of α. The enlargement of the region marked in panel (a) is shown in Fig. 6. The corresponding free-surface profiles at times (i)–(vi) marked in panel (c) are shown in Fig. 7.

required for the cylinder to complete one revolution. A similar mechanism is also responsible for the time evolution of film thickness shown in Fig. 3(a), where the load is too large to obtain a Moffatt-type smooth coating.

Due to gravity-driven drainage, excess liquid forms a bulge near the underside of the cylinder. When $A_0 < A_m^{\mathrm{Circular}}$, this bulge is carried around the cylinder in the direction of rotation with a

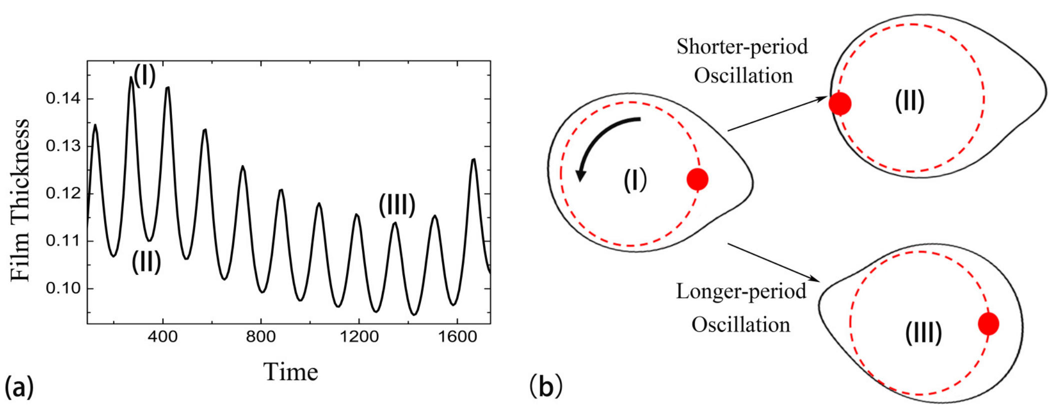

FIG. 6. (a) Enlargement of the region marked in Fig. 5(a). (b) Schematics of the free-surface profiles at times (I), (II), and (III) marked in panel (a). The red dots indicate the $\theta = \pi/2$ point on the cylinder surface (red dashed line).

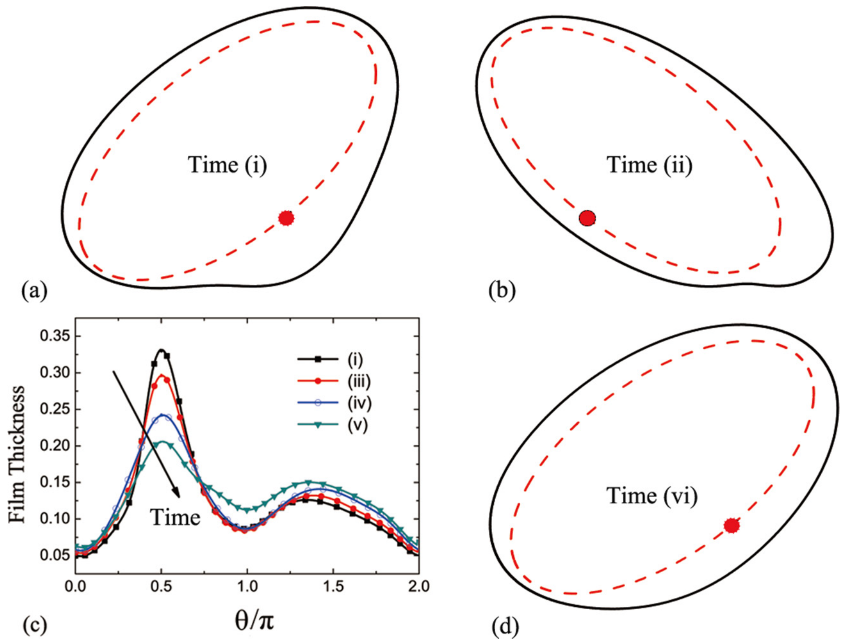

FIG. 7. (a), (b), (d) Free-surface profiles at three given times [marked in Fig. 5(c)]. (c) Film-thickness profiles in a rotating frame of reference at four given times [marked in Fig. 5(c)] with $\alpha = 0.5$, Bo $= 12.5$, $M = 0.1$, $W = 0.43$, and $A_0 = 0.72$. The red dots indicate the $\theta = \pi/2$ point on the cylinder surface.

speed that is slower than the speed of cylinder rotation, and the bulge shrinks in size with time [4]. The rotation of the bulge causes an oscillation in film thickness at $\theta = \pi/2$ [time (I) and time (III) in Fig. 6(b)] with a decaying amplitude and a longer period relative to the oscillation triggered by a nonuniform liquid distribution [time (I) and time (II) in Fig. 6(b)]. The resulting longer-period oscillation is superimposed on the shorter-period oscillation, causing the transient behavior shown in Fig. 5(a) to be different from that in the high-load case [Fig. 3(a)], where the bulge stays on the upward-moving side of the cylinder.

A similar time evolution of film thickness is also observed in the case where $\alpha = 0.8$ [Fig. 5(b)]. However, both the initial oscillation amplitude and the frequency of the longer-period oscillation are larger compared to the circular-cylinder case [Fig. 5(a)]. As will be shown later in this section, a smaller cylinder aspect ratio means that less liquid can be supported on the cylinder. As a consequence, a larger bulge will form at early times, and this explains the larger oscillation amplitude. Since a decrease in the cylinder aspect ratio also shortens the circumference of the cylinder, less time is required for the bulge to complete one revolution around an elliptical cylinder, which leads to a higher frequency of the longer-period oscillation in Fig. 5(b).

With a further decrease in α to a value of 0.5 [Fig. 5(c)], the oscillation amplitude decays almost monotonically, in contrast to the larger-aspect-ratio cases [Figs. 5(a) and 5(b)]. The coating reaches a quasisteady state within just ten revolutions, indicating a different mechanism underlying the shrinkage of the bulge. To investigate this, we select five times during the early transient stage [labeled (i)–(v) in Fig. 5(c)] and one time point during the quasisteady stage [labeled (vi) in Fig. 5(c)], and plot the corresponding film-thickness profiles and free-surface profiles in Fig. 7.

Figures 7(a) and 7(b) show that a liquid bulge forms on the upward-moving side of the cylinder due to gravity-driven drainage. The shape of the bulge varies to accommodate the variation in the cylinder orientation, but the bulge stays on the upward-moving side of the cylinder. Film thickness profiles at four times within the first four revolutions are shown in Fig. 7(c); the times are chosen so that the orientation of the cylinder is the same. The film thickness takes on its maximum value

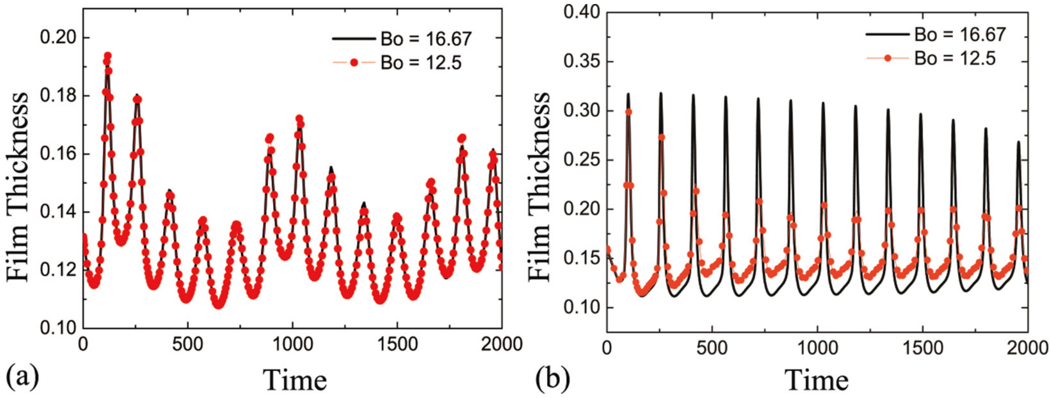

FIG. 8. Time variation of film thickness at $\theta = \pi/2$ for two different values of Bo with $M = 0.1$, $W = 0.43$, $A_0 = 0.72$ and (a) $\alpha = 0.8$ and (b) $\alpha = 0.5$.

in the bulge ($\theta = \pi/2$), which decreases monotonically in size after each revolution. This indicates that the liquid bulge on an elliptical cylinder can shrink in size even without rotating around the cylinder, in contrast to the circular-cylinder case. The mechanism underlying this phenomenon is discussed below. A comparison between Figs. 7(a) and 7(d) shows that liquid keeps being driven away from the bulge to the downward-moving side of the cylinder. As a consequence, a coating with relatively small variation in free-surface curvature (i.e., a smooth coating) can be obtained at a later time [Fig. 7(d)].

To understand the driving force behind the bulge shrinkage shown in Fig. 7(c), we plot in Fig. 8(b) the time evolution of film thickness at $\theta = \pi/2$ on an elliptical cylinder with $\alpha = 0.5$ for two different values of Bo. The time evolution of the film thickness on an elliptical cylinder with $\alpha = 0.8$ is shown in Fig. 8(a) for comparison. For $\alpha = 0.8$, varying Bo barely influences the coating evolution. This can be attributed to the fact that liquid bulge shrinks in size due to the rotation of the bulge, which redistributes liquid around cylinder, and surface tension plays a minor role in this process.

With a decrease in α to a value of 0.5 [Fig. 8(b)], the oscillation in film thickness becomes more pronounced (much larger oscillation amplitude), which indicates a larger liquid bulge forming during the early stages. In addition, the film-thickness evolution is highly sensitive to the value of Bo; a larger value of Bo leads to a smaller decay rate. Due to the increase in the bulge size, the viscous dragging caused by cylinder rotation is not strong enough to cause significant motion of the bulge when α is sufficiently small, so it stays on the upward-moving side of the cylinder [Figs. 7(a) and 7(b)]. Since surface tension makes a significant contribution to the film-thickness evolution only in regions where large variations in free-surface curvature occur [4] (i.e., the vicinity of the bulge), it tends to drive liquid away from the bulge, which eventually leads to a relatively smooth coating [Fig. 7(d)]. For this reason, a decrease in Bo, which corresponds to stronger surface-tension forces, enhances the damping of oscillations in film thickness [Fig. 8(b)], and thus shortens the time required to obtain the smooth coating.

A comparison between Fig. 4 ($A_0 = 0.72$) and Fig. 7(d) ($A_0 = 0.75$) shows that there exists a maximum load, $A_m^{\mathrm{Elliptical}}$, such that for $A_0 < A_m^{\mathrm{Elliptical}}$ a relatively smooth coating can be obtained on an elliptical cylinder. Since such coatings may be desired for many applications, it is important to characterize the behavior of the maximum load. To do so, we perform simulations by varying A_0 for given values of W, α, Bo, and M using initial condition (11). Oscillations in film thickness in the small-load cases should decay in amplitude (Fig. 5), while oscillations in the large-load cases should grow (Fig. 3).

For a circular cylinder, Moffatt [1] reported that there is a power-law relationship between the maximum load and the Stokes number, $A_m^{\mathrm{Circular}} \sim \gamma^{-1/2}$, where $\gamma = 1/MW$ is the Stokes number [Eq. (1)]. Kelmanson [3] pointed out that this power-law dependence holds only when γ is sufficiently

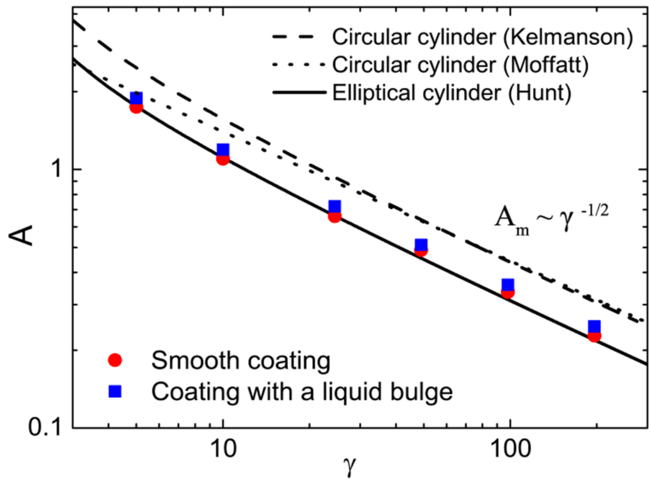

FIG. 9. Maximum load on an elliptical cylinder with $\alpha = 0.5$ and Bo = 12.5. Results of Moffatt [1], Kelmanson [3], and Hunt [9] are indicated by a dashed line, a dotted line, and a solid line, respectively.

large, and that Moffatt's criterion increasingly underestimates the maximum load with a decrease in γ. For elliptical cylinders, a similar power-law dependence is reported by Hunt [9] in the regime where surface tension and inertia are negligible.

Inspired by the above works, we plot the load, A, as a function of γ in Fig. 9 for $\alpha = 0.5$. The lower points (red circles) indicate the largest load that will result in a relatively smooth coating, and the upper points (blue squares) indicate the smallest load that will cause the growth of the liquid bulge. Results of Moffatt [1], Kelmanson [3], and Hunt [9] are shown in the same figure for comparison. As can be seen, our results agree well with those of Hunt.

For both a circular cylinder and an elliptical cylinder, Fig. 9 shows that increasing the Stokes number, which corresponds to stronger gravity-driven drainage, leads to a smaller maximum load. For a given value of γ, the maximum load on an elliptical cylinder is always smaller than that on a circular cylinder, but their ratio, $A_m^{\text{Elliptical}}/A_m^{\text{Circular}}$, is fairly constant (0.71) for $\alpha = 0.5$ over the range of γ investigated [9]. Both the circular and elliptical cylinders, there is approximately the same power-law dependence between the maximum load and γ, $A_m \sim \gamma^{-1/2}$.

The decrease in A_m can be rationalized by noticing that the liquid drainage rate is highly dependent on the orientation of the cylinder and the length of the minor axis, b. When the minor axis is perpendicular to the gravity vector, $\mathbf{g}$ (defined in Sec. II A), the liquid drainage rate takes on its maximum, and the maximum value itself increases with decreasing b. For a given value of cylinder rotation rate, a smaller cylinder aspect ratio, $\alpha = b/a$, gives rise to a larger mean rate of liquid drainage, and for this reason, less liquid can be supported on the cylinder.

In Fig. 9 results from Hunt's model and our model are in good agreement, despite the fact that effects of surface tension and centrifugal forces are neglected in Hunt's model. Good agreement is also observed in the case where $\alpha = 0.8$, but the results are not shown here for brevity. Based on these observations, we infer that for the parameter regime considered here, surface tension does not significantly influence the maximum load below which a relatively smooth coating can be obtained on an elliptical cylinder, but it does significantly influence the time needed to obtain such a coating [Fig. 8(b)].

C. Time-dependent cylinder rotation rate

When $A > A_m^{\text{Elliptical}}$, liquid tends to accumulate near the underside of the cylinder due to gravity-driven drainage, and the rate of liquid drainage is highly dependent on the orientation of the cylinder

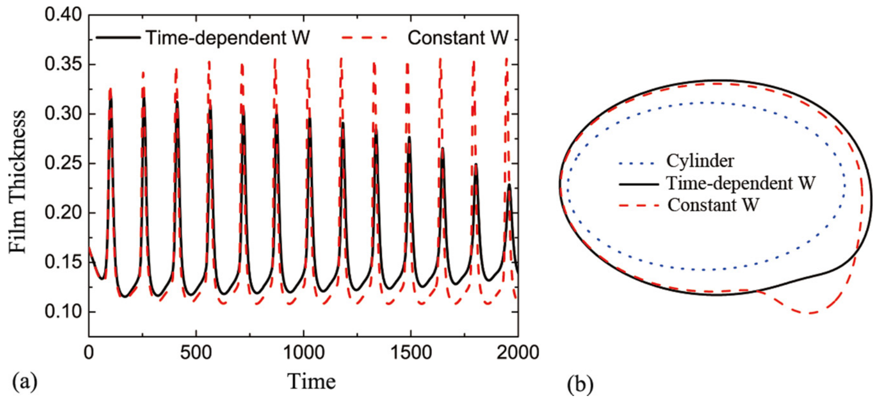

FIG. 10. (a) Time variation of film thickness at $\theta = \pi/2$ and (b) free-surface profiles at $t = 2000$ with $\alpha = 0.5$, Bo $= 12.5$, $M = 0.1$, $A_0 = 0.75$, and $W = 0.43$ (red dashed line) and $W = 0.43 - 0.11\cos(2{\times}0.043t)$ (black solid line).

(Fig. 4). We show in this section that varying the cylinder rotation rate based on cylinder orientation can allow us to obtain a relatively smooth coating with a mean rotation rate that is smaller than the critical value shown in Fig. 9.

For brevity, we consider the simplest case where the rotation rate, W, varies periodically as cylinder rotates,

$$W(t) = W_m - \delta\cos(2W_m Mt), \tag{16}$$

where W_m is a constant mean rotation rate and δ is a constant that sets the oscillation amplitude. This sinusoidal function basically ensures that the rotation rate takes on its minima ($W_m - \delta$) when the major axis is perpendicular to **g** and its maxima ($W_m + \delta$) when the major axis is parallel to **g**. We note that when the rotation rate is time-dependent, an additional term will appear in the momentum conservation equation [10]. However, when lubrication scales are used to estimate the strength of this term, it is multiplied by $\epsilon^2 Re_\Omega$ and so is neglected here (cf. Sec. II B).

To facilitate comparison with results obtained in the fixed-rotation-rate case when $\alpha = 0.5$ [Fig. 3(b)], we set $W_m = 0.43$ and $A_0 = 0.75$ ($> A_m^{\text{Elliptical}}$). Simulations were performed with different δ, and it was found that the liquid bulge will shrink in size when δ is sufficiently large. We pick $\delta = 0.11$ as a representative case and plot in Figs. 10(a) and 10(b) the time evolution of film thickness at the $\theta = \pi/2$ point on the cylinder surface and the free-surface profile in the quasisteady regime, respectively. Results from the constant-rotation case ($\delta = 0$) are shown in these two figures for comparison.

For $\delta = 0$ [red dashed line in Fig. 10(a)], the amplitude of the oscillation in film thickness increases with time until the coating reaches a quasisteady state in which a liquid bulge hangs from the underside of the cylinder [red dashed line in Fig. 10(b)]. For $\delta = 0.11$ [black solid line in Fig. 10(a)], the oscillation in film thickness decays in amplitude despite the fact that the given load is still larger than the critical value. The corresponding coating [black solid line in Fig. 10(b)] is close to a Moffatt-type smooth coating with a thicker film on the upward-moving side and thinner film on the downward-moving side. Simulations with even larger values of δ are beyond the capability of our simulations because extremely small time-step sizes are required. For this reason, whether there exits an upper limit for δ above which the bulge will grow is unknown.

We note that if the sign is changed in Eq. (16), the rotation rate will be minimized when the when the major axis is parallel to **g**. We found that in this case, the free-surface profile has a similar shape to that in the constant-rotation-rate case but with a slightly larger bulge. However, it is conceivable that there could be other cases where the coating is destabilized if the cylinder is oriented vertically for a long enough time.

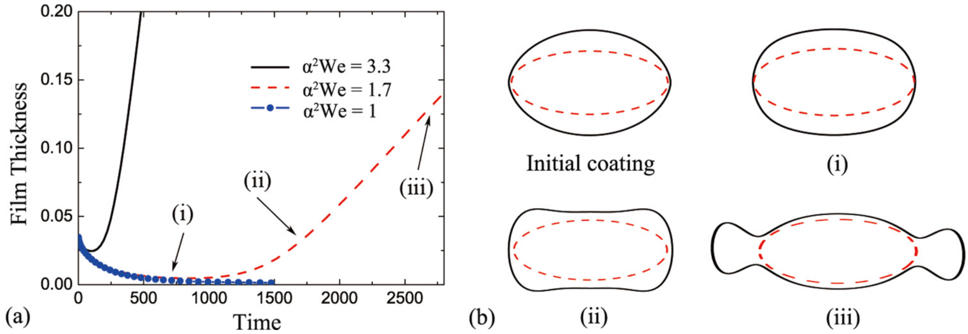

FIG. 11. (a) Time variation of film thickness at $\theta = 0$ (cylinder tip) with $A = 0.56$ for three different values of α^2We ($\alpha = 0.2$). (b) Initial coating and free-surface profiles at three given times [marked in panel (a)] with α^2We $= 1.7$.

IV. RESULTS: SMALL ASPECT RATIO

To consider the case where the cylinder aspect ratio is small (slender cylinder), we decrease α to a value of 0.2. With this aspect ratio, gradients in both centrifugal forces and substrate curvature become more significant relative to the $O(1)$-aspect-ratio case, and can adversely influence coating smoothness. As in the previous section, we first treat the case of a rapidly spinning cylinder where the effects of gravity can be neglected, and then consider the influence of gravitational forces.

A. Zero-gravity case

For an elliptical cylinder whose surface is described by Eq. (2), the substrate curvature reaches its maxima at the cylinder tips, $\kappa = \nabla_s \cdot \mathbf{n} = a/b^2$. An order-of-magnitude estimate of the strength of surface-tension forces is then $F_\sigma = \sigma a/b^2$. Liquid also experiences the strongest centrifugal forces over the cylinder tips, and an order-of-magnitude estimate of the strength of these forces is $F_\Omega = \rho\Omega^2 a^2$. Based on these observations, we characterize the strength of the centrifugal forces relative to surface-tension forces with the parameter $\alpha^2\text{We} = F_\Omega/F_\sigma = \rho\Omega^2 ab^2/\sigma$. For $O(1)$ values of the aspect ratio, $\alpha^2\text{We} \sim \text{We}$, which was the parameter used in Sec. III A. But for small aspect ratios, α^2We provides a better estimate of this force ratio.

For three different values of α^2We, simulations are performed with a moderate initial load, $A_0 = 0.56$, to ensure that film rupture (small A_0) and liquid shedding (large A_0) will not occur too early. The resulting time evolution of the film thickness at $\theta = 0$ (cylinder tip) is shown in Fig. 11(a).

For a moderate value of α^2We, the film thickness over the cylinder tip tends to decrease at early times but increase at later times, which we show in Fig. 11(a) with a red dashed line using $\alpha^2\text{We} = 1.7$ as a representative case. To gain deeper insight into the evolution of the coating, we select three times [marked (i)–(iii) in Fig. 11(a)], and plot the corresponding free-surface profiles in Fig. 11(b).

During relatively early times, surface-tension forces are stronger than centrifugal forces, and drive liquid away from the cylinder tips, which causes the decrease in the film thickness there. The resulting coating [time (i) in Fig. 11(b)] is thicker and almost flat on the top and bottom of the cylinder, but the free surface is still smooth. At later times, centrifugal forces dominate surface-tension forces in the thick-film region [i.e., the top and bottom of the cylinder in Fig. 11(b)] and tend to drive liquid back to the tips. This gives rise to four small liquid bulges located near the tips [time (ii) in Fig. 11(b)]. These small bulges are not stable and tend to merge to form two large bulges over the tips [time (iii) in Fig. 11(b)]. The resulting highly distorted interface shape significantly increases computational costs, and the simulation must be ended before the bulges would presumably break off.

A decrease in α^2We to a value of 1 [blue dotted line in Fig. 11(a)] strengthens surface-tension forces, so the film thickness over the tips decreases monotonically until it reaches zero. Film rupture

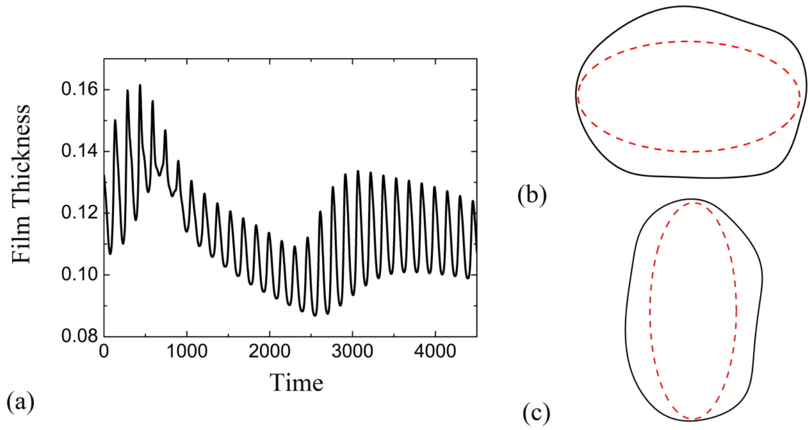

FIG. 12. (a) Time variation of film thickness at $\theta = \pi/2$ with $\alpha^2\text{Bo} = 2.5$, $W = 0.43$, $M = 0.1$, and $A_0 = 0.56 < A_m$. Corresponding free-surface profiles at (b) $t = 3323$ and (c) $t = 3531$.

is likely to occur in this case, leaving a bare substrate over the tips. With an increase in α^2We to a value of 3.3 [black solid line in Fig. 11(a)], stronger centrifugal forces on the liquid over the tips draw liquid from surrounding areas, which causes the film thickness to increase almost monotonically. As a result, liquid shedding may occur over the tips at a much earlier time relative to the case where $\alpha^2\text{We} = 1.7$. As noted in Sec. III A, similar phenomena are also observed for values of α as large as 0.95.

The results shown in Secs. III A and Secs. IV A indicate that for a rapidly rotating cylinder, the evolution of a thin-film coating can be highly sensitive to the value of α^2We. High values of α^2We may lead to film rupture over the tips, while low values of α^2We may result in liquid shedding. It is possible to obtain a smooth coating on a slender cylinder with moderate α^2We [time (ii) in Fig. 11(b)], but the liquid film would need to be solidified fast enough before small liquid bulges start to grow near the tips.

B. Gravity effects

We now include the effects of gravity and consider the constant-rotation-rate case first. An estimate of the importance of gravitational forces, F_g, relative to surface-tension forces, F_σ, is given by α^2Bo, which can be written as

$$\alpha^2\text{Bo} = \frac{F_g}{F_\sigma} = \frac{\rho g a}{\sigma a/b^2} = \frac{\rho g b^2}{\sigma}. \tag{17}$$

In our simulations, we set $M = 0.1$, $W = 0.43$, and $A_0 = 0.56 < A_m$, where $A_m = 0.57$ is the maximum load predicted by Hunt [9]. For these parameters, which characterize a rotating small-aspect ratio elliptical cylinder, we were unable to find quasisteady solutions regardless of the value of α^2Bo. For $\alpha^2\text{Bo} \gg 1$, liquid shedding is likely to occur at the cylinder bottom due to gravity-driven drainage, whereas for $\alpha^2\text{Bo} \ll 1$, film rupture is likely to occur at the cylinder tips due to the strong effects of surface tension.

For $\alpha^2\text{Bo} \sim 1$, where gravitational forces and surface-tension forces are in balance, the shape of the coating varies constantly as cylinder rotates and does not settle down to a Moffatt-type profile, in contrast to the $O(1)$-aspect-ratio case. We show in Fig. 12(a) the time evolution of the film thickness at the $\theta = \pi/2$ point on the cylinder surface. Free-surface profiles at two relatively late times when the major axis is perpendicular to **g** and parallel to **g** are shown in Figs. 12(b) and 12(c). Small liquid bulges form due to the combined effect of gravity [Fig. 7(a)] and surface tension [time (ii) in Fig. 11(b)]. These bulges rotate together with the cylinder and do not shrink in size during the time period we studied. Such bulges adversely impact coating smoothness and may be undesired for applications.

In the case where the cylinder rotation rate is time-dependent, high computational costs prevented us from running simulations with a high enough value of δ [variation in the rotation rate, Eq. (16)] to overcome gravity-driven drainage and obtain a smooth coating. To obtain a smooth coating on a small-aspect-ratio cylinder, one possible solution is to use a surfactant-laden liquid. In practice, surfactants are often present in coating liquids to control liquid wettability and surface tension. Since surfactant-induced Marangoni flows tend to weaken both gravity-driven drainage [16] and capillary flows [17], it is reasonable to expect that surfactant-induced Marangoni forces will drive liquid away from the bulges, leading to a smoother coating. For similar reasons, localized heating that drives a Marangoni flow from high- to low-temperature areas may also lead to a smoother coating.

V. CONCLUSIONS

The results of this work demonstrate that, in general, it is more difficult to obtain a relatively smooth coating on a rotating elliptical cylinder compared to a rotating circular cylinder. Curvature gradients on the cylinder surface lead to gradients in capillary pressure and centrifugal forces that make liquid distribution nonuniform. At relatively high rotation rates where the influence of gravity is negligible, even slight levels of cylinder eccentricity can significantly change the liquid distribution. For slender cylinders, coating evolution is very sensitive to the ratio of centrifugal and surface-tension forces. If this ratio is too small, film rupture will tend to occur at the cylinder tips, whereas if it is too large, liquid shedding will tend to occur there.

When the effects of gravity are significant, we have shown that the maximum load for which a relatively smooth coating can be obtained is smaller for elliptical cylinders [with $O(1)$ aspect ratios] compared to circular cylinders. In both cases, the maximum load decreases as the Stokes number increases with approximately the same power-law dependence. Our results represent an important extension of the work of Hunt [9] to account for the influence of surface tension. While surface tension does not significantly affect the maximum load condition for an elliptical cylinder (for the parameter regime considered here), it does significantly influence the time required to obtain a relatively smooth coating. Moreover, we also show that by applying a suitably chosen time-dependent rotation rate, more liquid can be supported on the cylinder than the maximum load predicted for constant rotation rates.

For slender cylinders (i.e., those with small aspect ratios) obtaining a relatively smooth coating is considerably more challenging due to the high interfacial curvature near the cylinder tips. Here it may be beneficial to introduce Marangoni stresses (via surfactants or temperature differences) to obtain a more uniform liquid distribution. Drying or solidifying the coating while simultaneously rotating the cylinder may also be an especially important strategy for obtaining a smooth coating.

ACKNOWLEDGMENTS

This work was supported through the Industrial Partnership for Research in Interfacial and Materials Engineering of the University of Minnesota. We are grateful to the Minnesota Supercomputing Institute (MSI) at the University of Minnesota for providing computational resources.

[1] H. K. Moffatt, Behaviour of a viscous film on the outer surface of a rotating cylinder, J. de Mécanique **16**, 651 (1977).

[2] V. V. Pukhnachev, Motion of a liquid film on the surface of a rotating cylinder in a gravitational field, J. Appl. Mech. Tech. Phys. **18**, 344 (1977).

[3] M. A. Kelmanson, Theoretical and experimental analyses of the maximum-supportable fluid load on a rotating cylinder, J. Eng. Math. **29**, 271 (1995).
[4] P. L. Evans, L. W. Schwartz, and R. V. Roy, Steady and unsteady solutions for coating flow on a rotating horizontal cylinder: Two-dimensional theoretical and numerical modeling, Phys. Fluids **16**, 2742 (2004).
[5] L. Preziosi and D. D. Joseph, The run-off condition for coating and rimming flows, J. Fluid Mech. **187**, 99 (1988).
[6] B. G. Zhang, D. E. Myers, G. G. Wallace, M. Brandt, and P. F. Choong, Bioactive coatings for orthopaedic implants-recent trends in development of implant coatings, Int. J. Mol. Sci. **15**, 11878 (2014).
[7] Y. Maeda, S. Miyoshi, and T. Yamaguchi, Oval cross section metal tube producing device and producing method, February 5, 2007, U.S. Patent No. 7,219,522.
[8] A. Thomas, Patterned chocolate coatings, methods, and apparatus for preparing same, June 26, 2001, U.S. Patent No. 6,251,455.
[9] R. Hunt, Numerical solution of the free-surface viscous flow on a horizontal rotating elliptical cylinder, Numer. Methods Partial Differ. Eqs. **24**, 1094 (2008).
[10] G. K. Batchelor, *An Introduction to Fluid Dynamics* (Cambridge University Press, Cambridge, 1967).
[11] M. A. Kelmanson, On inertial effects in the Moffatt-Pukhnachov coating-flow problem, J. Fluid Mech. **633**, 327 (2009).
[12] W. Li, M. S. Carvalho, and S. Kumar, Liquid-film coating on topographically patterned rotating cylinders, Phys. Rev. Fluids **2**, 024001 (2017).
[13] S. Dodds, M. S. Carvalho, and S. Kumar, Stretching and slipping of liquid bridges near plates and cavities, Phys. Fluids **21**, 092103 (2009).
[14] K. N. Christodoulou, S. F. Kistler, and P. R. Schunk, Advances in computational methods for free-surface flows, in *Liquid Film Coating*, edited by S. F. Kistler and P. M. Schweizer (Springer, Amsterdam, 1997), pp. 297–366.
[15] R. V. Roy, A. J. Roberts, and M. E. Simpson, A lubrication model of coating flows over a curved substrate in space, J. Fluid Mech. **454**, 235 (2002).
[16] D. E. Weidner, Suppression and reversal of drop formation on horizontal cylinders due to surfactant convection, Phys. Fluids **25**, 082110 (2013).
[17] W. Li and S. Kumar, Thin-film coating of surfactant-laden liquids on rotating cylinders, Phys. Fluids **27**, 072106 (2015).